Romanian Reports in Physics **76**, 506 (2024)

OPTICAL PROPERTIES OF Cu_2ZnSnS_4 AND Cu_2CdSnS_4 QUATERNARY COMPOUNDS

V. BATIR[1,*], V. ZALAMAI[2]

[1] Institute of Applied Physics, Moldova State University, 5 Academiei str., MD 2028, Chisinau, Republic of Moldova
[2] National Center for Materials Study and Testing, Technical University of Moldova, 78 31 August 1989 str., MD 2004, Chisinau, Republic of Moldova
[*] Corresponding author, Email: *valentinbatir@yahoo.com*

Received December 27, 2023

Abstract. Nowadays, the efficiency of Cu_2ZnSnS_4 (CZTS) thin-film solar cells is still limited by various factors such as: electronic disorder, secondary phases and the presence of antisite defects. In order to avoid this limitations, the Zn substitution by heavier atoms like Cd was proposed, as it may inhibit the formation of antisite defects, thereby increasing the minority carrier lifetime and reducing electronic disorder in the system. Thus, the main goal of this work was to investigate the optical properties of Cu_2ZnSnS_4 (CZTS) and Cu_2CdSnS_4 (CCTS) quaternary compounds. Hence, the reflectance, transmittance and photoluminescence spectra were recorded over a wide temperature range (from 10 to 300 K). As a result, for the CZTS sample, the optical band gap energy at room temperature was found to be equal to 1.46 eV. Also, reflectance and photoluminescence spectra at 15 K revealed essential details about the excitonic behavior in the CCTS sample, in particular for the A type exciton, with ground and excited states ($n^A = 1$ and $n^A = 2$) observed. The binding energy for the A type exciton was found to be 64 meV, leading to an estimated band gap width (E_g) of about 1.39 eV. In addition, at higher energies, spectra revealed maxima associated with the ground and excited states ($n^B = 1$ and $n^B = 2$) of the B type exciton, with an estimated binding energy of 75 meV and a continuum energy of about 1.51 eV.

Key words: Cu_2ZnSnS_4, Cu_2CdSnS_4, Tauc plot, band gap, optical properties, single crystals, reflectance spectra, photoluminescence spectra, excitons.

DOI: https://doi.org/10.59277/RomRepPhys.2024.76.506

1. INTRODUCTION

More and more attention is now being paid to the design and development of renewable energy sources, among which solar cells occupy a special place [1]. This, in turn, has led to the need for substantial research into the materials used for these applications. Particular attention is being paid to the development of low cost, environmental friendly and high efficiency solar cells [2, 3]. Among various types

of materials used or planned for use in solar cells a special interest recently take Cu_2ZnSnS_4 (CZTS), Cu_2CdSnS_4 (CCTS) and solid solutions on their basis which are supposed to be used in tandem solar cells. The potential application of multicomponent chalcogenide semiconductors in optoelectronics has also led to an increasing interest in the synthesis of these materials [4–7], which is not a trivial task and is connected to a several limitations, like secondary phases formation, lateral and bulk inhomogeneities, low energy for Cu_{Zn} and Zn_{Cu} antisite defects formation [8–11].

From the structural point of view, quaternary compounds are derived from ternary I-III-VI_2 compounds by replacing the group III atoms by II and IV atoms [12]. The ternary compounds in their turn are derived from binary II-VI compounds by replacing the group II atoms with a pair of group I and III atoms [12]. This atomic modifications result in increased chemical and structural flexibility in the ternary compounds, which show more variation in optoelectronic properties compared to the binary compounds. Further flexibility increase is achieved for the quaternary compounds, which can be adapted to applications in different photovoltaic technologies and for hydrogen evolution through the solar energy based water splitting [1, 13].

In this context, the quaternary compound CZTS is a promising light absorber material for use in solar cell fabrication, as it is composed of earth-abundant elements and has an optimum band gap of 1.5 eV with a high absorption coefficient of ~10^4 cm^{-1}. As a result, progressive power conversion efficiency (PCE) has been achieved since its first application in thin-film photovoltaics, increasing from 0.66 % to ~13.2 %, for a lithium-doped device [14].

However, the commercialization of CZTS solar cells is still limited as it has not reached the required PCE of 15% and is far from the theoretically calculated PCE of 35% [8]. This limitation is a consequence of the device open circuit voltage (V_{OC}) deficit, which was attributed to series of different limitations of the kesterite materials, including easy formation of Cu_{Zn} and Zn_{Cu} antisite defects due to close ionic radius and chemical-electronic properties of Cu^+ and Zn^{2+} cations [15].

To overcome this, cation substitution with larger atomic radius elements has been proposed [15, 16]. Since Cd is in the same group as Zn, it was chosen to replace zinc in CZTS material, resulting in the quaternary compound Cu_2CdSnS_4 (CCTS).

The CCTS has been relatively poorly studied and has drawn attention as a non-linear optical material for infrared devices [17] and as an absorbing layer for thin film solar cells [18]. By refining the technological parameters for growing CCTS crystals, photovoltaic devices with efficiencies of 12% have been achieved [19, 20]. In addition, the formation of Cu_{Cd} and Cd_{Cu} antisite defects reduces disorder and band tailing, due to the larger Cd ionic radius of 0.94 Å compared to Cu^+ and Zn^{2+}, which have an ionic radius of 0.74 Å [16, 21].

To date, insufficient investigation of the fundamental properties of this material, due to the difficulty in obtaining single crystal samples, hinders its further utilization. For example, knowledge of the optical properties of Cu_2CdSnS_4 compound is still

limited, relying mainly on a set of data related to thin film samples [22–24] and quaternary alloy nanostructures [25, 26]. This way, there is a lack of information regarding optical properties of this compound on single crystal samples. Also, values of the band gap width vary considerably, being enclosed in the interval of 1.35–1.45 eV [22–25], and are mainly determined by the absorption edge.

In this study, we have investigated the properties of the above-mentioned quaternary compounds by optical spectroscopy. We examined the reflectance, transmittance and photoluminescence spectra recorded over a wide temperature range (from 10 to 300 K) for single-crystal samples obtained *via* the chemical vapor transport method.

2. EXPERIMENTAL DETAILS

2.1. CRYSTAL GROWTH

The single crystals were obtained by the chemical vapor transport method (CVT) from high purity (99.999%) elemental components using 5 mg/cm^3 of iodine as the transport agent.

Initially, elemental components (copper, zinc, cadmium, tin and sulphur), weighted in proportions corresponding to the stoichiometric composition, were used as starting materials for the synthesis of polycrystalline quaternary compounds by solid state reaction.

In the next step, polycrystalline ingots were ground and loaded into quartz ampoules, which were then placed in a horizontal two-zone furnace. The ampoules were evacuated to a residual pressure of ~10^{-3} Pa, the internal diameter was ~16–22 mm while the length was ~170 mm.

In order to form metal iodides and to clean the ampoules from possible uncontrolled crystallization centers, the reaction zone was heated to 670 K, while the crystallization zone was heated to 740 K. The ampoules were held at these temperatures for 2–3 days, after which the temperature in the zones was equilibrated across the ampoule and kept at 970 K for 24 h.

Afterwards, the temperature in the reaction zone was then gradually increased to 1070 K (over 170 h) and the growth process lasted for 240 h.

2.2. MEASUREMENTS PERFORMING

The elemental composition of the single crystals was determined from X-ray fluorescence spectra using the “X-Calibur” Xenemetrix system. The instrument is equipped with a X-ray source with Rh target and a SDD detector with a resolution of 135 keV. Calculation of the composition was performed by using an integrated software.

Reflectance and transmittance spectra at room temperature were measured using a dual-beam spectrophotometer Jasco V670, enabling the acquisition of absolute values for the reflection and transmission coefficients in a spectral range from 620 to 1240 nm. Low-temperature spectra were obtained from samples placed within a sealed helium cryostat LTS-22 C 330 optical cryogenic system, using a standard monochromator MDR-2 (with an aperture ratio of 1:2 and a linear dispersion of 7 Å/mm). Photoluminescence spectra were measured with a double-beam spectrometer SDL-1, featuring an aperture ratio of 1:2 and a linear dispersion of 7 Å/mm, and excited by a 325 nm He-Cd laser line. The majority of measurements were conducted with entrance and exit slits of the spectrometer not exceeding 50 μm, yielding a resolution of approximately 0.5 meV.

3. RESULTS AND DISCUSSION

3.1. SAMPLES DESCRIPTION AND CHEMICAL COMPOSITION

The crystals had relatively small dimensions, approximately 1–2 mm width by 3–5 mm length, with one mirror-like surface of good optical quality (Fig. 1). The reverse side of the crystals featured an uneven surface, making it difficult to measure transmittance spectra due to light scattering from the backside of the samples.

In order to avoid this difficulty, the largest CZTS crystal was selected for the measurements (Fig. 1b). As a result, transmittance spectra could only be measured for the CZTS sample and not for the CCTS compound, due to the small size of the crystals of the later compound.

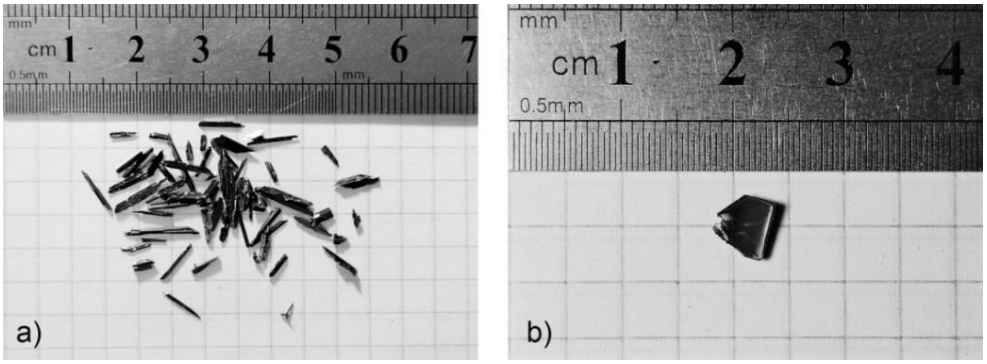

Fig. 1 – Photo of single crystals obtained by the chemical vapor transport method:
a) CCTS and b) CZTS.

The composition values obtained for the CZTS and CCTS samples are presented in Table 1. Thus, the CZTS sample is Cu-rich and Zn-poor, whereas

the CCTS sample is Cu-poor and Cd-poor. Also, the S content is rich for both samples.

Table 1

The XRF elemental analysis of CZTS and CCTS single crystals.
Note: II = Zn or Cd, M = Cu + II + Sn

Sample	Cu (at.%)	Zn (at.%)	Cd (at.%)	Sn (at.%)	S (at.%)	Cu/ (II + Sn)	II/ Sn	M/ S
CZTS	18.4	8.6	–	9.1	63.9	1.04	0.95	0.57
CCTS	17.2	–	9.1	9.6	64.0	0.92	0.96	0.56

3.2. REFLECTANCE AND TRANSMITTANCE SPECTRA OF CZTS SAMPLE

Figure 2 illustrates the reflectance and transmittance spectra of the CZTS sample. In the reflectance spectra, two maxima labeled A1 and B1 are observed at 1.375 and 1.700 eV, respectively. These maxima are attributed to direct transitions between conduction band C_1 and valence bands V_1 and V_2, which are split by the crystal field and the spin-orbital interaction [27]. In the transmittance spectrum, at an energy of 1.466 eV, the crystal ceases to transmit light. However, due to the poor quality of the side opposite to the mirror-like surface (as it was mentioned above), the transmission coefficient of such a sample did not exceed 1.5%. Thus, the changes in the current transmittance spectrum should be considered rather than its absolute values.

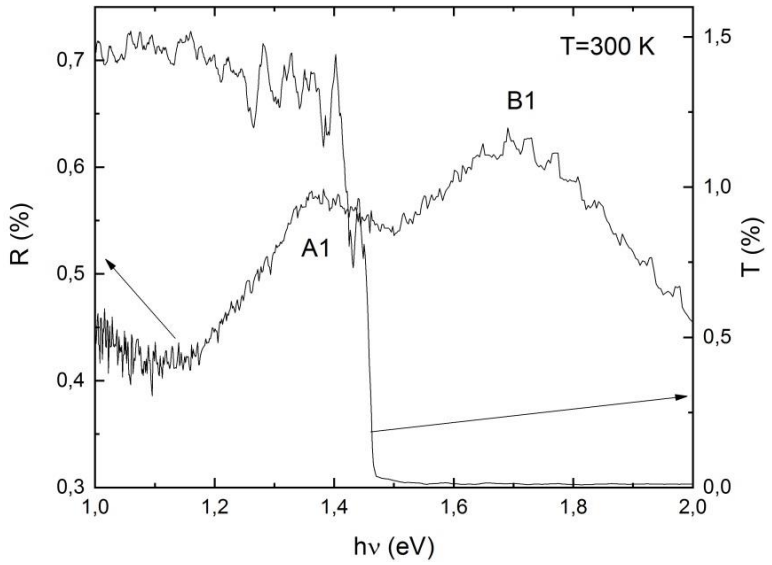

Fig. 2 – The reflectance and transmittance spectra of CZTS sample measured at room temperature.

As is well-known for direct band gap semiconductors, the square of the absorption coefficient is proportional to the band gap energy. By plotting the dependence of $(\alpha h\nu)^2$ on energy and performing a linear approximation of the linear region, the energy of the band gap can be determined by extrapolating to the ordinate axis. This method is known as the Tauc plot and was proposed by the Czech physicist Jan Tauc [28].

In this work, the absorption spectrum of the CZTS sample (Fig. 3) was obtained by using the following formula:

$$\alpha = \frac{1}{d}\ln\left(\frac{(1-R)^2}{T}\right), \tag{1}$$

where R, T and d represent the reflectance, transmittance and the thickness of the sample, respectively.

The spectrum presented in Fig. 3 corresponds to room temperature of the sample and is characterized by a sharp onset of the fundamental absorption, which is associated with the relatively thick sample (about 2 mm). The onset of the edge absorption is observed at an energy of ~1.4 eV, which is quite close to the band gap energy of this material [29].

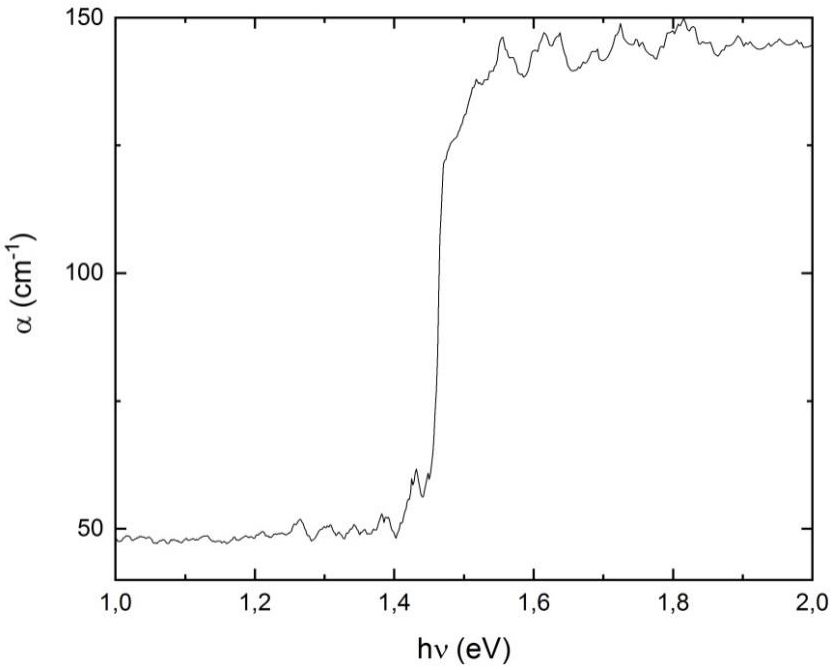

Fig. 3 – The absorption spectrum of CZTS sample obtained at room temperature.

Figure 4 illustrates the dependence of the square of the absorption coefficient on the energy of the light and shows a linear approximation of the characteristic region. The optical band gap energy of this material at room temperature was found to be 1.455 eV. This value is comparable to those obtained by spectroscopic ellipsometry and spectrophotometry analysis [30, 31].

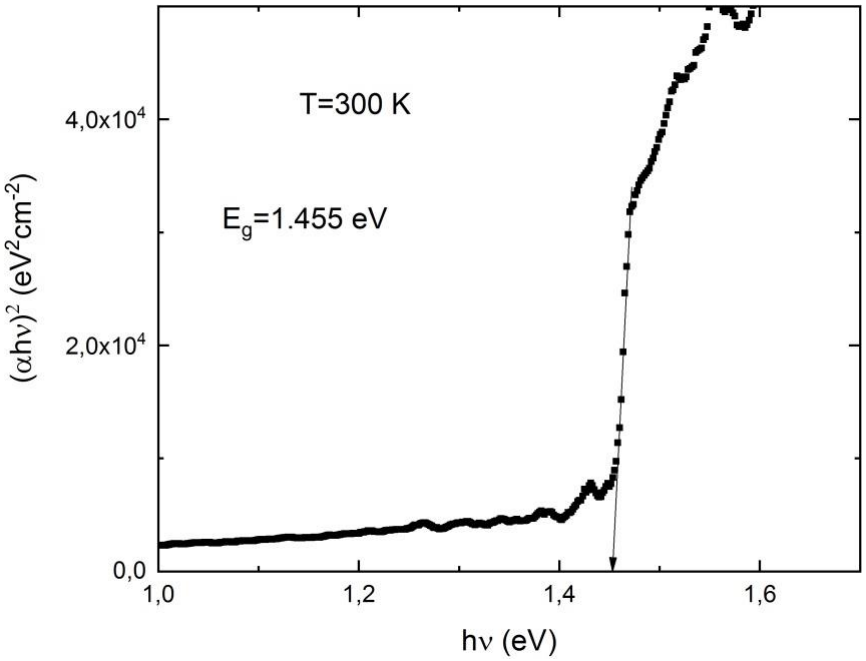

Fig. 4 – The dependence of $(\alpha h\nu)^2$ on energy for CZTS sample and the estimation of the optical band gap energy (E_g) using the Tauc plot [29].

An interesting pattern emerges when studying the behavior of reflectance spectra from the monocrystalline CZTS sample. Figure 5 shows reflectance spectra measured over a temperature range of 10–300 K. Unfortunately, due to the high concentration of intrinsic defects, which is characteristic for a kesterite type compounds, it is not always possible to clearly identify the maxima in the reflectance spectra. As shown in Fig. 5, two maxima, labeled A1 and B1, are present in the spectra at all temperatures. The temperature dependence of maxima position is more clearly illustrated in the inset of Fig. 5. In particular, the shift for the B1 maximum is more pronounced than that for the A1 maximum. The fact that the A1 and B1 maxima behave similarly with temperature suggests that the transitions occur between the same conduction band minimum and different valence band maxima, which are C_1, V_1 and V_2, as proposed above.

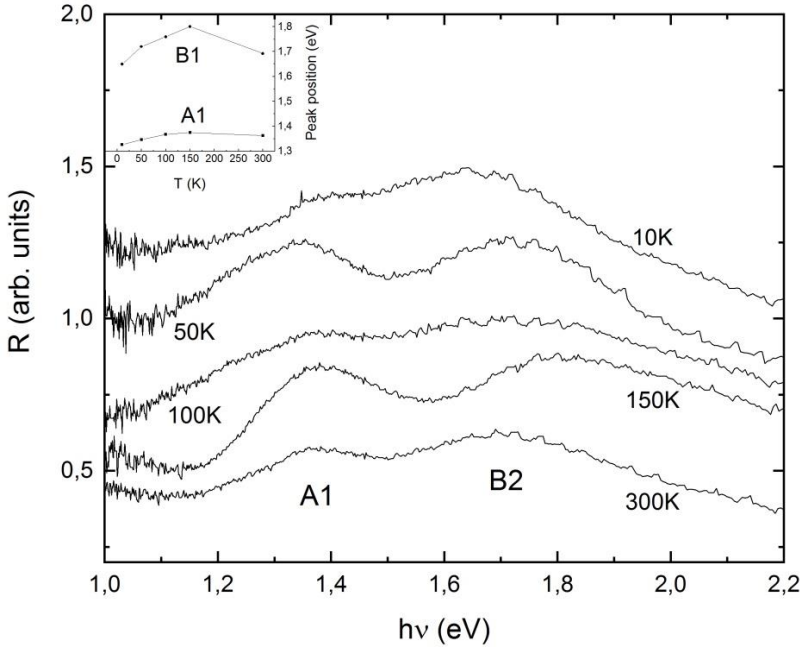

Fig. 5 – Reflectance spectra of the single crystal CZTS sample measured at different temperatures. The inset graph shows the change in maxima position with temperature.

3.3. REFLECTANCE AND PHOTOLUMINESCENCE SPECTRA OF CCTS SAMPLE

In the reflectance spectra of CCTS single crystal sample (Fig. 6), only the A1 maximum is observed over the whole temperature range. The B1 maximum was not detected, but a broad C1 maximum is visible at higher energies (2.27 eV at 300 K). The C1 maximum is very broad and asymmetric and may include the B1 maximum. Also, from inset graph (Fig. 6), it can be noticed that behavior of C1 maximum with temperature is typical; it shifts towards higher energies as the temperature decreases. It is most likely associated with direct transitions between the conduction and valence bands, but occurring at different points in the Brillouin zone. Thus, the A1 maximum is observed as a shoulder in the spectra, while the C1 maximum is very broad, making it somewhat difficult to determine its exact position.

Figure 7 shows the reflectance (R) and photoluminescence (PL) spectra near the interband gap measured at a temperature of 15 K. In the reflectance spectra, both the ground and excited states of the A exciton are observed. For the A exciton, the ground state ($n^A = 1$) is located at 1.326 eV. In the photoluminescence spectrum, besides the ground state of the A exciton, an excited state ($n^A = 2$) is observed at 1.374 eV. In addition, a narrow maximum around 1.358 eV is observed in the PL spectrum, which can be associated with the longitudinal exciton ω_L, while the ground state ($n^A = 1$) observed in both R and PL spectra corresponds to the transversal exciton ω_T.

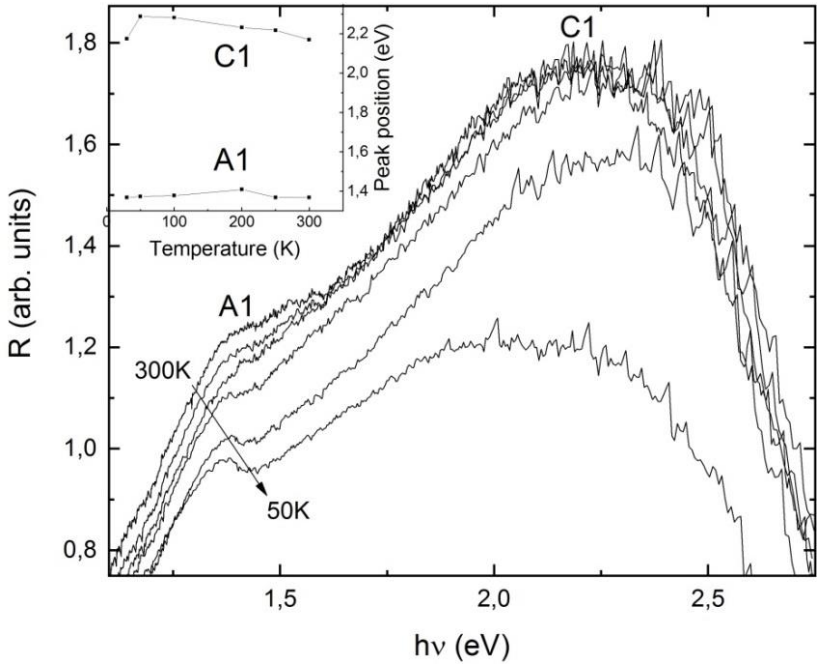

Fig. 6 – Reflectance spectra of CCTS sample measured at different temperatures. The inset graph shows the change in maxima position with temperature.

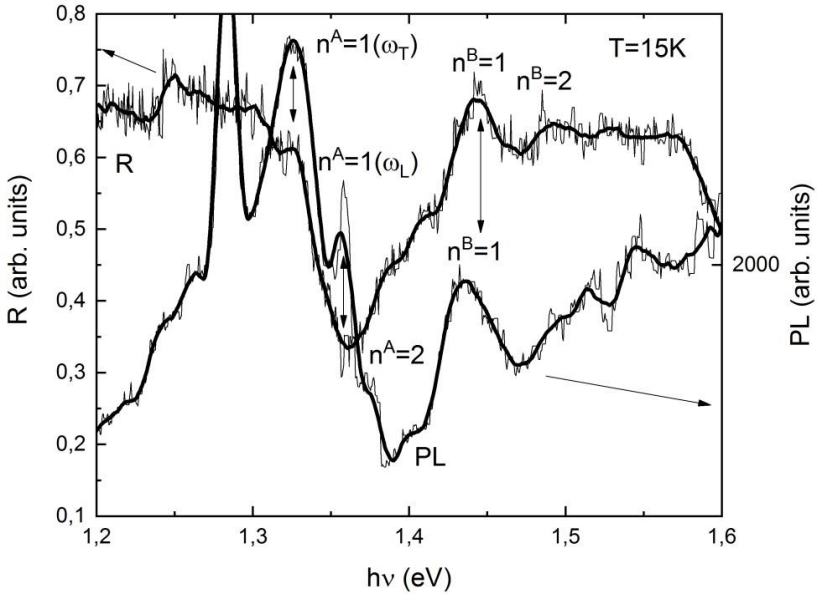

Fig. 7 – Reflectance (*R*) and photoluminescence (PL) spectra measured at a temperature of 15 K in the absorption edge region for the monocrystalline CCTS sample.

From the positions of the ground and excited states of the A exciton, the Rydberg constant (Ry) and the band gap (E_g) can be estimated using the following expressions:

$$\mathrm{Ry} = \frac{n_2^x\left(E_2 - E_1\right)}{\left(\frac{n_2}{n_1}\right)^x - 1}, \tag{2}$$

$$E_g = \frac{E_2\left(\frac{n_2}{n_1}\right)^x - E_1}{\left(\frac{n_2}{n_1}\right)^x - 1}, \tag{3}$$

here $n_1 = 1$ is the ground state of the exciton equal to energy E_1, $n_2 = 2$ represents the excited state of the same exciton equal to energy E_2 and x is a constant assumed to be equal with 2 [32].

For the A exciton, Ry is 64 meV. Knowing the Rydberg constant, it is easy to estimate the band gap width (E_g), which is about 1.39 eV. Obtained value is slightly lower to the once obtained for the thin film samples [27], but is in good agreement with the literature value obtained for bulk polycrystalline samples and measured by different techniques [33].

Furthermore, in the reflectance and photoluminescence spectra at higher energies, maxima corresponding to the ground ($n^B = 1$) and excited ($n^B = 2$) states of the B exciton are observed. The ground state ($n^B = 1$) is located at an energy of 1.434 eV, while the excited state ($n^B = 2$) is located at 1.490 eV. Based on these data, the Rydberg constant (Ry) for the B exciton is estimated to be 75 meV. Consequently, the continuum energy for the B exciton is 1.51 eV.

Figure 8 shows the band structure of a CCTS compound as calculated in the study [27]. The band structure shows that the material is a direct band gap semiconductor and the minimum direct transitions occur at the Γ point of the Brillouin zone. In addition, direct transitions may also occur at other points of the Brillouin zone (Z, P and Y). The arrows in Fig. 8 indicate possible direct transitions.

Considering the band structure shown in Fig. 8, in the region of the interband gap located at the Γ point, the presence of three branches in valence band (V_1, V_2 and V_3) can be observed. These branches are split by the crystal field and the spin-orbital interaction. Thus, from the analysis of the band structure, reflectance and photoluminescence spectra, it can be concluded that the A exciton is formed by an electron from the lower conduction band C_1 and a hole from the upper valence

band V_1. The B exciton state is formed by an electron from the conduction band C_1 and a hole from the second valence band V_2. Due to the high concentration of free carriers, the observed contours of the excitonic reflectance spectra differ considerably from the classical ones due to the screening effect.

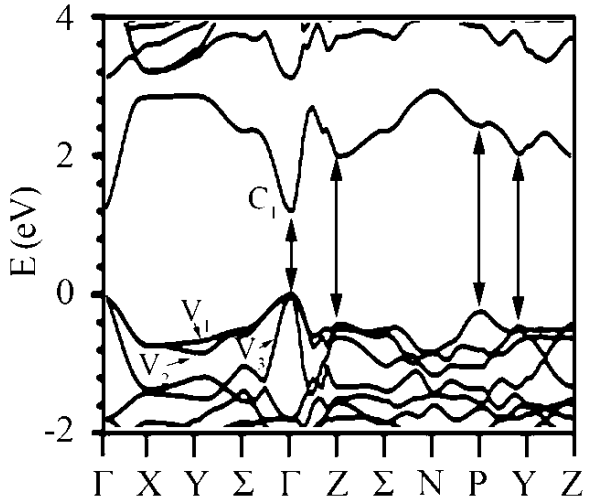

Fig. 8 – The band structure of the CCTS compound at different points of the Brillouin zone [27].

4. CONCLUSIONS

Single crystals of both Cu_2ZnSnS_4 and Cu_2CdSnS_4 have been investigated by measuring reflectance, transmittance and photoluminescence spectra over a wide temperature range (from 10 to 300 K).

As a result of using the Tauc plot, the optical band gap width for the CZTS sample, determined at room temperature, is 1.46 eV.

Additionally, two types of excitons, A and B, were identified in the reflectance and photoluminescence spectra. For both types of excitons, ground states (n = 1) and excited states (n = 2) were observed and their binding energies were determined. For the A type exciton the binding energy is 64 meV while for the B type it is 75 meV. Also, the band gap width for the CCTS compound, determined at the temperature of 15 K, is 1.39 eV.

In the photoluminescence spectra, maxima associated with transversal (ω_L) and longitudinal (ω_T) excitons were observed at energies of 1.326 and 1.328 eV, respectively. It was established that the A type exciton is formed by electrons from the conduction band C_1 and holes from the valence band V_1. At the same time, the B type exciton is formed by the same electrons and holes from the V_2 valence band. Thus, taking into account the calculated binding energies of the excitons

(Rydberg constant), it has been estimated that the splitting of the valence bands V_1 and V_2 is equal to 125 meV.

Acknowledgements. This work was supported by the National Agency for Research and Development of the Republic of Moldova under the projects: ANCD 22.80013.5007.5BL and ANCD 20.80009.5007.03. The author is also very grateful to Prof. I. V. Bodnar and Senior Researcher I. A. Victorov for obtaining the monocrystalline samples by the chemical vapor transport method. Special thanks to L. Dermenji for measuring the elemental composition of the single crystal samples.

REFERENCES

1. W. Wang, M. T. Winkler, O. Gunawan, T. Gokmen, T. K. Todorov, Y. Zhu, and D. B. Mitzi, Adv. Energy Mater. **4**, 1301465 (2013).
2. W. J. E. Beek, M. M. Wienk, and R. A. J. Janssen, Adv. Mater. **16**, 1009 (2004).
3. E. D. Kosten, J. H. Atwater, J. Parsons, A. Polman, and H. A. Atwater, Light Sci. Appl. **2**, e45 (2013).
4. H. Katagiri, K. Jimbo, S. Yamada, T. Kamimura, W. S. Maw, T. Fukano, T. Ito, and T. Motohiro, Appl. Phys. Express **1**, 041201 (2008).
5. S. Schorr, G. Wagner, M. Tovar, and D. Sheptyakov, MRS Proc. **1012**, 1012 (2007).
6. O. V. Parasyuk, I. D. Olekseyuk, and L. V. Piskach, J. Alloys Compd. **397**, 169 (2005).
7. H. Matsushita, T. Maeda, A. Katsui, and T. Takizawa, J. Cryst. Growth **208**, 416 (2000).
8. S. Giraldo, Z. Jehl, M. Placidi, V. Izquierdo-Roca, A. Pérez-Rodríguez, and E. Saucedo, Adv. Mater. **31**, 1806692 (2019).
9. S. Hadke, W. Chen, J. M. R. Tan, M. Guc, V. Izquierdo-Roca, G.-M. Rignanese, G. Hautier, and L. H. Wong, J. Mater. Chem. A **7**, 26927 (2019).
10. S. Schorr, G. Gurieva, M. Guc, M. Dimitrievska, A. Pérez-Rodríguez, V. Izquierdo-Roca, C. S. Schnohr, J. Kim, W. Jo, and J. M. Merino, J. Phys. Energy **2**, 012002 (2020).
11. R. Fonoll-Rubio, J. Andrade-Arvizu, J. Blanco-Portals, I. Becerril-Romero, M. Guc, E. Saucedo, F. Peiró, L. Calvo-Barrio, M. Ritzer, C. S. Schnohr, M. Placidi, S. Estradé, V. Izquierdo-Roca, and A. Pérez-Rodríguez, Energy Environ. Sci. **14**, 507 (2021).
12. S. Schorr, Thin Solid Films **515**, 5985 (2007).
13. Tsuji, Y. Shimodaira, H. Kato, H. Kobayashi, and A. Kudo, Chem. Mater. **22**, 1402 (2010).
14. J. Zhou, X. Xu, B. Duan, H. Wu, J. Shi, Y. Luo, D. Li, and Q. Meng, Nano Energy **89**, 106405 (2021).
15. S. Bourdais, C. Choné, B. Delatouche, A. Jacob, G. Larramona, C. Moisan, A. Lafond, F. Donatini, G. Rey, S. Siebentritt, A. Walsh, and G. Dennler, Adv. Energy Mater. **6**, 1502276 (2016).
16. J. Li, D. Wang, X. Li, Y. Zeng, and Y. Zhang, Adv. Sci. **5**, 1700744 (2018).
17. K. A. Rosmus, J. A. Brant, S. D. Wisneski, D. J. Clark, Y. S. Kim, J. I. Jang, C. D. Brunetta, J.-H. Zhang, M. N. Srnec, and J. A. Aitken, Inorg. Chem. **53**, 7809 (2014).
18. S. Hadke, S. Levcenko, G. Sai Gautam, C. J. Hages, J. A. Márquez, V. Izquierdo-Roca, E. A. Carter, T. Unold, and L. H. Wong, Adv. Energy Mater. **9**, 1902509 (2019).
19. C. Yan, K. Sun, J. Huang, S. Johnston, F. Liu, B. P. Veettil, K. Sun, A. Pu, F. Zhou, J. A. Stride, M. A. Green, and X. Hao, ACS Energy Lett. **2**, 930 (2017).
20. Z. Su, G. Liang, P. Fan, J. Luo, Z. Zheng, Z. Xie, W. Wang, S. Chen, J. Hu, Y. Wei, C. Yan, J. Huang, X. Hao, and F. Liu, Adv. Mater. **32**, 2000121 (2020).
21. K. C. Nwambaekwe, V. S. John-Denk, S. F. Douman, P. Mathumba, S. T. Yussuf, O. V. Uhuo, P. I. Ekwere, and E. I. Iwuoha, J. Mater. Res. Technol. **12**, 1252 (2021).
22. H. Guo, Y. Li, X. Fang, K. Zhang, J. Ding, and N. Yuan, Mater. Lett. **162**, 97 (2016).
23. Tombak, T. Kilicoglu, and Y. S. Ocak, Renew. Energy **146**, 1465 (2020).
24. H. Guan, J. Zhao, X. Wang, and F. Yu, Chalcogenide Lett. **10**, 367 (2013).

25. Y. Al-Douri, A. A. Odeh, M. R. Johan, Z. Z. Chowdhury, R. F. Rafique, A. H. Reshak, and C. H. Voon, Int. J. Electrochem. Sci. **13**, 6693 (2018).
26. A. Odeh, Y. Al-Douri, R. M. Ayub, M. Ameri, A. Bouhemadou, D. Prakash, and K. D. Verma, Appl. Phys. A **122**, 888 (2016).
27. N. Sarmadian, R. Saniz, B. Partoens, and D. Lamoen, J. Appl. Phys. 120, 085707 (2016).
28. J. Tauc, Mater. Res. Bull. **3**, 37 (1968).
29. M. Pilvet, M. Kauk-Kuusik, M. Altosaar, M. Grossberg, M. Danilson, K. Timmo, A. Mere, and V. Mikli, Thin Solid Films **582**, 180 (2015).
30. S. Levcenko, E. Hajdeu-Chicarosh, E. Garcia-Llamas, R. Caballero, R. Serna, I. V. Bodnar, I. A. Victorov, M. Guc, J. M. Merino, A. Pérez-Rodriguez, E. Arushanov, and M. León, Appl. Phys. Lett. **112**, 161901 (2018).
31. S.-Y. Li, C. Hägglund, Y. Ren, J. J. S. Scragg, J. K. Larsen, C. Frisk, K. Rudisch, S. Englund, and C. Platzer-Björkman, Sol. Energy Mater. Sol. Cells **149**, 170 (2016).
32. N. N. Syrbu, V. V. Ursaki, *Exciton polariton dispersion in multinary compounds*, in: R. M. Bergin (ed.), *Exciton Quasiparticles: Theory, Dynamics and Applications*, Nova Science Publishers Inc., New York, 2011, pp. 1–130.
33. S. Levcenko, S. S. Hadke, L. H. Wong, and T. Unold, Phys. Rev. Mater. **5**, 104605 (2021).